SynthETC: A Statistical Model for Severe Winter Storm Hazard on Eastern North America

Timothy Hall
NASA Goddard Institute for Space Studies
New York, NY
timothy.m.hall@nasa.gov

James F. Booth
City College of the City University of New York

Abstract

We develop, evaluate, and apply "SynthETC," a statistical-stochastic model of winter extra-tropical cyclones (ETCs) over eastern North America. SynthETC simulates the life cycle of ETCs from formation to termination, and it can be used to estimate the probability of extreme ETC events beyond the historical record. Two modes of climate variability are used as independent covariates: El Niño/Southern Oscillation (ENSO) Niño3.4 and the monthly North Atlantic Oscillation (NAO). We use SynthETC to estimate the annual occurrence rate over sites in eastern North America of intense ETC passage in different ENSO and NAO states. Positive NAO is associated with increased rates over the North Atlantic, while negative NAO is associated with decreased rates over the North Atlantic and increased rates over northern Quebec. Positive ENSO is associated with decreased rates over the North Atlantic, Ontario, and the Canadian Maritime, while negative ENSO is associated with increased rates over those regions, as well as the Great Lakes region.

1. Introduction

Winter extra-tropical cyclones (ETCs) pose a major hazard to eastern North America. These storms can cause damage through their precipitation, e.g., blizzards and floods, and through their winds, e.g., extreme surface winds and storm surge. Heavy snowfall causes power outages, collapse of structures, and suspension of travel and commerce. ETC winds sometimes reach hurricane force and drive damaging coastal storm surge. Orton et al. (2016) found that in the New York City area, ETCs are the dominant cause of surge events that have annual probability greater than 1%. NOAA's NCDC estimated $40.9 billion in insured and uninsured losses due to ETC events from 1980 to 2016 that caused more than one billion dollars in damage each (www.ncdc.noaa.gov/billions/summary-stats; see also Smith and Katz, 2013).

ETCs are a dominant source of mid-latitude weather, and their varied formation and evolution mechanisms have been studied using a wide range of observational, theoretical, and modeling approaches (reviewed in Catto, 2016). The characterization of ETC variability in the Northeast US has been documented for some time (e.g. Miller 1946), and a climatology of northeast ETC tracks exists (Hirsch et al. 2001). However, our understanding of the link between the storms' variability, hazardous extreme events, and large-scale climate variability remains incomplete (Colle et al. 2015). An examination of ETC tracks on seasonal timescales suggests that there are a large set of forcing parameters, however the variance

explained by multiple predictors is less than 50% (DeGaetano 2008). Climatologically, ETC tracks have been used to identify a preferred track path for storms that create wind hazards in the northeast (Booth et al. 2015). However, the probabilistic analysis in that work is limited by the short time span of the reanalysis utilized. A large body of work on case studies has led to a general appreciation of snow storms in the region (Kocin and Uccellini, 2002), but the distinction between these case studies and all other ETC tracks has not been made.

There has also been work examining the link between ETC paths and planetary scale climate variability (i.e., teleconnections patterns) for the Northeast region. Eichler and Higgins (2006) composited track density by phases of El Niño/Southern Oscillation (ENSO), and Grise et al (2013) composited by ENSO, the North Atlantic Oscillation (NAO), the Pacific North American pattern (PNA), and the Madden-Julian Oscillation (MJO) separately. DeGaetano et al. (2002) used a discriminant forecasting procedure to find heightened ETC activity over the U.S. east coast for positive ENSO and NAO states. Berhardt and DeGaetano (2012) used seasonal averages of ETC tracks to show that storm surge is more likely to occur in the region during ENSO positive years concurrent with NAO negative years. However, the statistical significance in their analysis is limited by the small number of times those two events have occurred at the same time for the time period used in the Berhardt and DeGaetano (2012) study: 1951-2006. Ning and Bradley (2015) found regional correlations between extreme winter precipitation over the northeastern U.S. and southeastern Canada and ENSO, the NAO, and the PNA. Their work focused on the

precipitation events only, and so there is still a need to explore the three-part link between the teleconnection patterns, the ETC paths, and the resulting hazards.

Multiple approaches to understand the connections between storms and hazards exist, including case-study analysis, numerical modeling, and statistical modeling. Our work here utilizes statistical modeling. Such an approach has been adopted widely for tropical cyclones, for both commercial and academic applications (e.g., Vickery et al., 2000; James and Mason, 2005; Emanuel et al., 2006; Rumpf, et al., 2007; Hall and Jewson, 2007; Hall and Yonekura, 2013; Yonekura and Hall, 2014; Bonazzi et al., 2014). Additionally, a statistical downscaling approach has been utilized substantially in Europe for windstorms (Klawaand Ulbrich, 2003; Haas and Pinto 2012; Born et al., 2012; Seregina et al., 2014), and to a lesser extent in North America as well (He et al. 2010). While these studies focus on ETC-related hazards, the statistical models are not built around the cyclone paths or storm tracks. The statistical modeling of Eulerian storm tracks (Compo and Sardeshmukh, 2004; Ambaum and Novak, 2014; Yang et al. 2015) helps explain the physics of the storm tracks on seasonal time scales. However they do not offer distinct information about ETC tracks. Gaffney et al. (2006) developed regression-mixture models of existing ETC tracks, and used the models to cluster the tracks based on their trajectory (regardless of location). The model/cluster analysis was useful for assessing the skill of a GCM in generating ETC tracks. However, the model was not designed to generate synthetic ETC tracks. Hunter et al. (2016) used ETC tracks to build an

aggregate risk model and found that including both the frequency and intensity information improved the model skill.

A major goal of our effort is to quantify the rate of extreme ETC events on local regions throughout eastern North America, including events that have not occurred historically. There are various statistical approaches possible. The advantage of a statistical track model compared to approaches that emphasize local historical occurrence is that information from the entire domain is exploited for the local rate estimation. This is particularly valuable for estimating rates for events that have never occurred historically and/or for estimating rates in combinations of climate indices for which there are few historical instances. In effect, the large synthetic event set increases the precision of rate estimates. While the complexity of generating synthetic storm sets may introduce bias, Hall and Jewson (2008) showed for tropical cyclones that the gain in precision outweighs the potential loss in accuracy.

2. Data

The Bauer et al. (2016) cyclone tracking algorithm (MCMS) was applied to 1979-2015 ERA-Interim reanalysis (Dee et al. 2011) sea level pressure (SLP) data to generate global ETC tracks based on the position of the ETC central pressure minimum. ERA-Interim has been shown to be as good or better than other existing reanalyses for tracking ETCs in the Northern Hemisphere (Hodges et al. 2011). The

120 decision to use data for 1979 onward is based on the improved skill in the
121 reanalyses in the satellite era.
122
123 A regional subset of the tracks was defined as all tracks that had at least one 6-
124 hourly position within the region spanning: 110°W by 45°W and 25°N by 65°N.
125 Using all months of the year, this regional subset contained 12049 tracks. We refer
126 to these as the "historical" data. They are comprised of 6-hourly values of storm
127 center position and central pressure. Most of the storms are weak disturbances. We
128 are most interested in simulating intense ETCs. To this end, we filter the historical
129 ETCs: 1. We remove tropical cyclones (TCs), by removing tracks that closely match
130 HURDAT (Landsea et al., 2015), in terms of location of the storm center during the
131 track evolution; and 2., keep only the remaining ETC tracks whose central pressure
132 (CP) for at least one point along the track falls 35mb or lower ("35mb+") than the
133 local annual-cycle SLP climatological value at that point. We will also refer to these
134 as strong, or intense, cyclones, and we refer to the CP deficit from local climatology
135 as the intensity of the storm. To create the climatology, we first create daily data by
136 averaging the SLP from 00, 06, 12 and 18Z. The daily data is averaged from 1979 -
137 2015 and then smoothed using a 30-day running mean. This provides a daily
138 climatological value for SLP at each latitude/longitude location that is subtracted
139 from the 6-hourly SLP for each cyclone center, providing measure of cyclone
140 intensity based on the SLP anomaly. The total number of 35mb+ storms is 1782, and
141 these storms comprise the training dataset for SynthETC. This is a sufficient number
142 of events for model training, more than twice as many, in fact, as the number of

143 events used successfully in the tropical cyclone model training of Hall and Jewson
144 (2007).
145
146 MCMS identifies tracks based on the depressions in SLP. But the initial location and
147 the termination location are primarily determined based on existence of a local
148 minimum in SLP. The tracker performs as well as alternate existing tracking
149 algorithms (Bauer et al. 2016), and includes data regarding a region of influence of
150 each cyclone. However, we here use only the track data. All trackers have some
151 difficulty detecting cyclones in regions of steep terrain (Neu et al. 2013), and
152 therefore we do not focus on the area near the Rockies.
153
154 Fig 1 shows the 1979-2015 35mb+ historical ETC tracks; that is, the 1979-2015 ETC
155 tracks whose CP for at least one point along the track is at least 35mb lower than the
156 local SLP. Fig 2 shows the monthly histogram of storm frequency for the full set, the
157 full ETC set (minus TCs), and the 35mb+ ETC set. While the full set has little annual
158 cycle, the set of intense ETCs strongly peaks in winter, dropping nearly to zero in
159 summer. This is consistent with the seasonality of the strength of the baroclinicity.
160 The 35mb value is the approximate minimum threshold that excludes the vast
161 majority of summer storms.
162
163 The independent variables in our analysis are 1979-2015 monthly time series of
164 ENSO and NAO. For ENSO we use the monthly Niño3.4 SST index available on
165 NOAA's ESRL website (www.esrl.noaa.gov/psd/gcos_wgsp/Timeseries/Nino34),

which is derived from HadISST1 gridded SST data (Rayner et al., 2003). For the NAO we use the monthly index available from the Climate Research Unit of the University of East Anglia (crudata.uea.ac.uk/cru/data/nao/nao.dat), which is derived from SLP differences between Iceland and the Azores and Gibraltar (e.g., Jones et al., 1997).

3. Model

In developing SynthETC we aim to model ETC tracks stochastically from formation through termination. The goal is twofold:

1. To construct an ETC "event set", much larger than the historical set, that has the statistical properties of the historical set. The large synthetic set allows more precise estimates of rates of rare events than estimates based solely on the historical storms, and allows estimation of the probability for events that have not occurred historically.
2. To estimate the impact of NAO and ENSO on the occurrence rates of extreme ETCs. These indices are dominant modes of climate variability, and have been shown to influence winter ETC frequency (e.g., DeGaetano et al., 2002), although they are by no means the only factors (Grise et al., 2013; Yang et al., 2015). Additional covariates could be tested and utilized. However, for seasonal and longer-term probabilistic hazard modeling (as opposed to a nearer-term operational modeling) our covariate selection is strongly

188 influenced by parsimony and by the requirement that covariate forecasts be
189 available for seasonal forecasting.
190
191 SynthETC is based on 37 years of reanalysis track data, 1979-2015. To estimate
192 return periods of events well beyond 37-years the model assumes that 1979-2015 is
193 statistically representative of much larger time periods; that is, that the ETC
194 statistics are stationary. SynthETC provides rates of rare events that haven't
195 occurred in the historic 1979-2015 record, but would happen eventually if the
196 1979-2015 period were repeated many times. There is evidence for non-stationarity
197 in ETC meteorology, for example, an increased frequency and northward shift in the
198 mean storm track (e.g., Voce et al., 2014). Such signals are not currently included in
199 SythETC, though the model could be used to explore the impact of secular changes
200 in mean track or cyclogenesis rates and locations on extreme storm statistics.
201
202 Our modeling approach is similar to Hall and Jewson (2007) and Hall and Yonekura
203 (2013) for tropical cyclones. SynthETC consists of four components: 1. formation, 2.
204 propagation, 3. termination, and, 4. central pressure. Formation, propagation, and
205 termination are modeled via local regression, while central pressure is modeled
206 using a weighted sampling scheme. We review the components briefly here, and
207 refer readers to Hall and Yonekura (2013) for additional methodological details.
208
209 **3.1. Formation**

210 At each point on a 1° by 1° grid, Poisson regression is performed in which the
211 dependent variable is the monthly number of 35mb+ ETCs originating "near" the
212 grid point, and the independent variables are monthly NAO and ENSO indices. In
213 order to focus on cold-season storms we use only the months October through April
214 in the time series, which capture the vast majority of 35mb+ ETCs (Fig. 2). "Near" is
215 determined by the Gaussian weighting kernel used in the calculation of the
216 regression coefficients. The weight of a formation event to the regression declines
217 with distance from the point according to a Gaussian kernel. The bandwidth of the
218 kernel (140km) is determined by drop-one-year out-of-sample likelihood
219 maximization. The result of the regression at each location is a Poisson mean rate
220 for the number of ETCs formed monthly within Oct-Apr as a function of NAO and
221 ENSO for the weighted area about the grid point. This rate is then scaled down to
222 the grid box area by the ratio of the grid-box area to the weighted area under the
223 kernel. The formation rate dependence on ENSO and NAO is illustrated and
224 discussed in Section 4.2.
225
226 Once the monthly rates are estimated, seasonality needs to be accommodated, so
227 that, for example, October rates are appropriately different than January rates for
228 the same NAO and ENSO values. A kernel pdf in formation location and pentad-of-
229 year is constructed with optimized bandwidths of 140 km and 15 days. At each
230 location the pentad-of-year dependence is normalized and then multiplied by the
231 monthly rate from the Poisson regression at that location, resulting in a pentad
232 Poisson rate consistent with the date, as well as NAO and ENSO. Fig 3 shows the

spatial map of the kernel pdf for the central pentad of each of the 12 months of the year. The bulk of formation for these intense ETCs occurs in the winter off the US eastern seaboard, typical of nor'easters. There are also pockets of activity in the Midwest, particularly over the Great Lakes (Sanders and Gyakum, 1980).

Formation occurs during simulations as follows: During each pentad of year at each 1°-by-1° site, the ENSO and NAO values for the current simulation month are combined with the regression coefficients to determine the monthly Poisson rate. The rate is multiplied by the pentad-of-year pdf for the site, and the resulting Poisson distribution is sampled to determine how many formation events have occurred.

To examine uncertainty in formation ENSO and NAO dependence due to the finite (37 year) data record we perform a bootstrap analysis on the Poisson regression for the domain-wide Oct-Apr 35mb+ formation count. The best estimate difference between the most (ENSO=-2 and NAO=+2 in units of standard deviations) and least (ENSO=+2 and NAO=-2) active states is 31 storms annually Oct-Apr (60 compared to 29). The 5%-95% confidence limits on this difference over the bootstrap set is 38 to 23. Thus, while there is considerable uncertainty in the mean rate's ENSO and NAO sensitivity, the sign of the sensitivity is robust. In future analysis we plan to perform such bootstrap analysis on all components of the model.

3.2. Propagation

Tracks are simulated in 6-hour increments. Given a simulated ETC center at position **x**(t) we determine its position at **x**(t+6hr) by analyzing the propagation of "nearby" (defined below) historical ETCs. A set of 6-hourly latitude and longitude increments from the historical ETCs is constructed, and these increments are regressed on three covariates: NAO, ENSO, and an annual cycle of 500mb NCEP winds. The coefficients resulting from the regression are combined with the current values of the covariates in the simulation to generate the mean 6-hourly simulation track increment from **x**(t). "Nearby" is defined by a Gaussian weighting kernel; that is, the contribution of historical track increments to the regression at **x**(t) declines with distance from **x** according to this kernel. The bandwidth of the kernel, 200 km, is determined by drop-one-year-out out-of-sample forecast error minimization.

Treatment of the residuals from the regressions is an important part of the simulations. It constitutes the stochastic component of the track model. The residuals are standardized assuming a non-isotropic correlated bi-normal distribution whose coefficients (x and y variances and co-variances) are calculated from analysis of nearby historical residuals. Once standardized, the two directions can be modeled independently as a lag-one auto-regressive process, AR(1), whose autocorrelation coefficient is calculated from analysis of nearby historical standardized anomalies. Performing a simulation increment thus consists of drawing a random normal, obtaining standardized anomalies from the AR(1) model, dimensionalizing and rotating the anomalies using the variances and co-variances to obtain residuals, adding the means, and finally updating the position of the

280 simulated track. More details can be found in Hall and Jewson (2007) and Hall and
281 Yonekura (2013).
282
283 Fig 4 illustrates the track calculation, showing a four-day mean track launched from
284 an arbitrary point (72°W, 36°N). The figure also shows 1000 tracks launched from
285 the same point and date, now fully simulated with the stochastic component.
286 Although the general orientation is similar, there is considerable spread of the
287 stochastic tracks about the mean track, indicating that much of the track variance is
288 unexplained by the covariates (ENSO, NAO, 500mb annual cycle winds). The set of
289 1979-2015 historical tracks that originate near the launch point (shown in blue)
290 appears as a typical subset of the much larger synthetic set.
291
292 **3.3. Termination**
293
294 At each six-hour time step starting at step 6 (1.5 days) of a track simulation a
295 random number is drawn and compared to a termination probability. If the
296 probability exceeds the draw, then the track is terminated. The probability, P, is the
297 fraction of nearby historical track points that are terminal; i.e., P equals the
298 weighted sum of terminal points divided by the weighted sum of all points, where
299 the weighting kernel is Gaussian with a 150km bandwidth. The 1.5-day onset of
300 termination is chosen to mimic the duration distribution of the historical ETCs, for
301 which 1.5 days is the shortest track. The resulting simulation and historical track-

duration frequency distributions match closely, and the mean simulation track duration is 4.5 days, compared to 4.8 days for the historical set.

3.4. Intensity

Intensity is simulated by weighted random sampling of historical intensity time series; i.e., time series of SLP local climatology minus CP. Once a track is simulated we select from the set of historical intensity time series a single time series to place on the simulated track. The selection is weighted towards historical intensity series whose associated tracks are "similar" to the simulated track in question. "Similar" is defined by a set of bandwidths associated with the Gaussian weighting kernels of the criteria. The criteria are the date of year, duration of track, and locations of track formation, mid-point, and termination. This scheme results in a selected intensity time series similar, though not generally identical, in start date and duration to the simulation track. The intensity series is then shifted and scaled in time to match the start date and duration of the simulation track. An example of out-of-sample intensity simulation on a historical track from 2012 is shown in Fig 5 using sampling data from 1979-2015 that excludes 2012. In this example seven historical intensity time series have probabilities greater than 0.001 of being selected, with the most probable having 0.45. During simulations the sampling scheme selects a single time series, most commonly the series with the highest probability, but sometimes one with lower probability.

Hunter et al. (2016) found evidence for a correlation between track density and intensity, and concluded that much of the relationship was driven by the mutual dependence of both variables on several modes of climate variability, including NAO. In our intensity-sampling scheme, dependence of intensity on ENSO and NAO is indirect. ENSO and NAO influence the formation region and track shape, and these, in turn, influence the intensity time-series selection. If the physical relationship between NAO-ENSO and ETCs has a signature in both intensity and formation or track, then an NAO-ENSO-intensity relationship will be captured by our sampling scheme.

Once the weighted random sampling is performed, the lifetime maximum intensity (LMI) along the track receives a small random perturbation so that simulated LMIs are not limited to historical values. The perturbations are drawn from a generalized extreme value fit of the historical LMIs to ensure that the distribution of the perturbed set conforms closely to that of the unperturbed set.

In this initial development of the model, we have chosen to use CP deficit with respect to local SLP as the measure of storm intensity. This is due to its simplicity and the fact that it is a reasonable proxy for the SLP gradient around the storm, which drives cyclonic winds. Other measures of storm strength are relative vorticity at 850 hPa (e.g., Hoskins and Hodges 2002) and the strength of surface winds. However, with these there is a question of what region around the storm to use, or what horizontal resolution to consider when calculating the vorticity. Sanders and

Gyakum (1980) defined storm intensification based on a change in SLP normalized to a fixed latitude. Because the focus here is intensity and not intensification, the CP difference from climatology is used to remove the effects of latitudinal variation in climatological SLP (see Ulbrich et al. 2009 for more discussion). However, a relationship between latitude and intensity does exist, with stronger storms occurring further north. We attribute this primarily to the fact that ETCs in our study region typically travel north and strengthen during their life cycle, e.g., Hoskins and Hodges (2002). There may also be some bias with respect to latitude in our intensity metric, due to the absence of explicit inclusion of the Coriolis parameter's dependence on latitude, which affects the geostrophic wind-pressure relationship. Future work with the model will be dedicated to testing the impact of different metrics of storm intensity, including synthetic wind fields.

4. Simulations and Analysis

We perform two classes of simulations: 1. 1000 repeat simulations of the 1979-2015 historical period (37,000 yrs), driven by the historical ENSO and NAO time series; and 2. 10,000-yr simulations with ENSO and NAO held constant in each of 25 combinations of ENSO = -2, -1, 0, +1, +2 and NAO = -2, -1, 0, +1, +2 in units of standardized anomalies. The first set is used to evaluate the model against historical diagnostics and to estimate average occurrence rates of extreme ETC events. The second set is used to estimate the impact of ENSO and NAO on extreme event occurrence rates.

Fig 6 shows tracks from four sample simulations of 1979-2015 and can be compared to Fig 1. The overall shape and distribution of the historical tracks are well captured by the simulations. The majority of intense ETCs in the historical data and the simulations occur over the North Atlantic. However, there are occurrences of 30mb+ and even 60mb+ intensity extending into the U.S. northeast and Canadian Maritimes.

SynthETC provides a way to estimate probabilities of extreme events that are well beyond the historic record. Fig 7 shows three examples of synthetic ETCs that pass within 200km of Washington DC, New York City, and Boston with intensity greater than 60mb, having peak intensities of 71mb, 67mb, and 60mb, respectively. Frequency analysis of the 37,000-year synthetic set reveals that ETCs with 60mb+ intensity passing within 200km of Boston, New York City, and Washington DC have average return periods of 96 yrs, 308 yrs, 2018 yrs, respectively. Finally, occurring 8 times in the synthetic set (average return period of 2800yrs) is an ETC with 60mb+ intensity within 200km of all three cities. Such a storm would devastate the US east coast, shutting down economic activity for many days and potentially causing power outages for millions of people.

4.1. Model Evaluation

To evaluate the model we compare values of diagnostics derived directly from the historical ETCs to the distribution of values derived from the ensemble of simulations. A necessary condition for a stochastic model to be unbiased is that the diagnostic value (e.g., track flux across constant longitude lines) derived from the historical ETC data should be a typical member of the set of diagnostic values from the simulations. Fig. 8 shows the number of tracks crossing lines of constant longitude and latitude. For most regions the historical curve falls inside the spread of simulation curves, consistent with a lack of bias. An exception is at high Arctic latitudes, where the model underestimates eastward propagation. This region is outside our primary area of interest.

To evaluate the model further, we calculate the return periods as a function of intensity of ETCs passing within 200km of nine US cities: New York New York, Boston Massachusetts, Washington DC, Toronto Ontario (Canada), Chicago Illinois, Detroit Michigan, Montreal Quebec (Canada), Halifax Nova Scotia (Canada), and Duluth Minnesota (Fig 9). The spread of return period curves across the 1000 simulations of 1979-2015 bounds the curve obtained from the historical data in most regions and intensities, again consistent with a lack of bias. When the simulations are placed in series, intensity values at return periods beyond the 37-year duration of the historical data can be estimated. For example, the analysis indicates that an ETC with intensity greater than 60mb within 200km of New York is about 308-year event and within 200km of Boston about a 96-year event. (See also Fig. 7.) Neither such event occurs in the 37-year historical record.

4.2. ENSO and NAO Dependence

We use the model to estimate the dependence of regional extreme ETC annual rate as a function of ENSO and NAO. The model is run for 10,000 years each for 25 fixed combinations of ENSO and NAO: ENSO=-2,-1,0,+1,+2 and NAO=-2,-1,0,+1,+2 in standardized units. The synthetic storms for each multi-year simulation are then used to compute a map of the annual probability of occurrence within 200km of an ETC with 50mb+ intensity. Fig 10 shows these spatial maps for nine ENSO-NAO combinations, and Fig 11 shows the fractional change with respect to the neutral (0,0) state. Figs 12 and 13 show the effects of NAO-ENSO on ETC formation rates and tracks separately. These figures illustrate properties of model mean rates that are well converged due to the large number of simulation years. Uncertainties on these mean rates due to the choice of the training data and choices in modeling schemes will be explored in future work.

Positive NAO is associated with an increased rate of passage of severe ETC (50mb+ intensity) in the North Atlantic (NA) and a decreased rate over the mid-latitude Atlantic and northern Quebec, and negative NAO is associated with the opposite (Fig. 11). There is also a smaller region of enhanced ETC passage rate over the US mid-Atlantic states for positive NAO. The increased NA rate for positive NAO is consistent with increased formation to the southwest over the Canadian maritime and Canadian Midwest (Fig 12). However, the increased ETC rate in northern

Quebec for negative NAO has no such negative-NAO formation increase to the southwest. The Quebec increase can, however, be understood in terms of the NAO influence on tracks. Fig 13 shows mean tracks of fixed duration (16 time steps or 4 days) launched from three points in nine ENSO and NAO combinations. Negative NAO is associated with slower (i.e., shorter in Fig 13) continental tracks that are more prone to curve north into northeastern Canada before reaching the NA, resulting in increased passage in that region. Similarly, tracks originating at lower latitude are slower and more zonal, and there is an increase in ETC occurrence in the Atlantic at mid latitudes for NAO negative. By contrast, for positive NAO the tracks are straighter, northeastward oriented, and faster, enhancing the higher NA rates (Figs 10, 11).

The NAO dependence is largely consistent with past studies. Serreze et al. (1997), Pinto et al. (2009), Grise et al. (2013) and Hunter et al. (2015) examined the effect on ETCs of the NAO (and other climate modes) using varying domain definitions and track datasets. All four studies found increased (decreased) NA track density and decreased (increased) subtropical and mid-latitude Atlantic track density during positive (negative) NAO, similar to the anomalies of Fig 11. The results here are also consistent with Gaffney et al (2007), who classified ETC tracks using a clustering analysis. Gaffney et al (2007) found that northeastward straight and fast tracks (their "D cluster") occurred preferentially during positive NAO phases, while the slower, eastward tracks occurred preferentially during negative NAO phases, similar to the more southern mean track dependence of Fig 13.

462

463 However, our result of increased rate of severe ETCs over northern Quebec for
464 negative NAO is at odds with Grise et al. (2013). The reasons for the difference are
465 unclear, but we note that the metrics are not strictly comparable, as we restrict
466 attention to extreme storms defined by CP deficit, while Grise et al. uses a surface
467 relative vorticity threshold. Our negative-NAO northward tracks are reminiscent of
468 the northward "V cluster" of Gaffney et al (2007), whose preferential SLP anomaly
469 pattern has some overlap with negative NAO. Serreze et al (1997) also inferred a
470 positive winter ETC anomaly for negative NAO over northern Labrador and Quebec.
471 Our result of increased rates over the U.S. upper Midwest and Ontario for low NAO
472 is consistent with the negative correlation between extreme precipitation and NAO
473 in that region found by Ning and Bradley (2015).

474

475 ENSO is associated with severe ETC rate anomalies distinct from NAO. Rates are
476 lower (higher) for positive (negative) ENSO over the NA and northeastern Canada,
477 reaching into the northeast US and the upper US Midwest. Unlike the northern
478 Quebec feature for the NAO, the ENSO effects can be explained qualitatively by
479 anomalies in formation. Positive (negative) ENSO is associated with a swath of
480 decreased (increased) formation across the US Midwest, northeast and NA that is
481 upstream of regions of decreased (increased) passage rates (Fig. 12). Compared to
482 NAO, ENSO has a smaller effect on mean tracks, though there is a shift to more zonal
483 propagation during positive ENSO (Fig 13) consistent with a more robust zonal jet, a
484 shift that modifies the spatial distribution of passage rates.

The ENSO dependence is also consistent with past studies. *Grise et al*. (2013) saw an increase (decrease) in ETC track density and formation over a swath of area including the US Midwest, northeast, and the NA for lower (higher) ENSO anomaly. They also saw the opposite sign effect to the south of this swath, which is hinted at in our Fig 11 by the small blue (red) patches in the mid-latitude Atlantic indicating decreased (increased) passage rate for lower (higher) ENSO. (This regional effect is weaker in our analysis because of the restriction to intense ETCs.) A similar pattern in track-density was found by Eichler and Higgins (2006) and Plante et al. (2015). Plante et al. (2015) in particular observed a distinct increased occurrence of intense ETCs (by vorticity) over the Great Lakes region for negative ENSO, consistent with our results in Fig 11. Ning and Bradley (2015) also found a negative ENSO-extreme winter precipitation correlation over the northern Great Lakes region. Finally, Degaetano (2008) observed that El Niño is associated with increased US east-coast frequency for all winter storms, but that there is little effect for strong storms, again consistent with our results. Note that track-density and precipitation as a metric is sensitive to ETC propagation and formation. By contrast, the analysis here isolates the ENSO influences on formation and propagation, revealing a larger effect via formation than propagation.

In some regions ENSO and NAO can combine to increase rates more than either alone. For the Great Lakes region and northern Quebec the combination of negative ENSO and negative NAO results in a sharp increase in rate of intense ETC passage.

508 For the New York and southern New England region negative ENSO and positive
509 NAO maximize the rate. These sensitivities are illustrated in Fig 14 at Duluth and
510 New York City. Over Duluth there is a factor of eight minimum-to-maximum
511 variation in annual passage rate of 50mb+ intensity ETCs (0.004-0.03 yr^{-1}) from
512 ENSO and NAO = -2, -2 to +2, +2. Over New York City the variation is a factor of four
513 (0.012-0.05 yr^{-1}). Berhardt and DeGaetano (2012) found increased US northeast
514 storm surge occurrence for positive ENSO and negative NAO, a combination that we
515 find results in a negative extreme ETC rate anomaly in the region. This is not
516 contradictory, however, because the focus of Berhardt and DeGaetano (2012) was
517 storm propagation speed. The enhanced surge was associated with slower moving
518 ETCs, which we see in negative NAO (Fig 13), and which also tend to be weaker.
519
520 **5. Conclusions**
521
522 We have developed, evaluated, and applied "SynthETC", a new statistical-stochastic
523 model of ETC hazard for Eastern North America. The model simulates the life cycle
524 of ETCs from formation to termination, using central pressure deficit from local SLP
525 climatology as the measure of intensity. SynthETC can be used to estimate the rates
526 of events on local regions, including unlikely but severe events that may not have
527 occurred in the historical record. Model evaluation shows that SynthETC matches
528 well (and extends) ETC occurrence statistics on a range of eastern North American
529 sites. Generation of large synthetic ETC event sets is an approach to winter-storm
530 hazard assessment that is consistent with hurricane hazard assessment in the

commercial catastrophe modeling industry (e.g., Bonazzi et al., 2014). We are currently working to develop wind fields to go along with the synthetic track and pressure time series, clearly necessary to translate severe ETC occurrence rates to wind and storm surge hazard.

SynthETC uses two key modes of natural climate variability as independent covariates: ENSO and the NAO. We find regional severe ETC passage-rate sensitivities to ENSO and NAO that are largely consistent with past studies using different methodologies. ENSO can be forecast skillfully months in advance. It is natural to ask, therefore, if SynthETC could be used to make probabilistic seasonal forecasts of ETC hazard. We are planning tests to determine whether such forecasts are skillful.

Acknowledgements

This work was supported by the NASA IDS grant "Vulnerability of the U.S. Atlantic Coast to Hazards Associated with Extreme Winter Storms" (NNX14AD48G) and NASA MAP grant "Subpolar North Atlantic Air-Sea Fluxes Associated with Mid-Latitude Cyclones and their Effect on AMOC" (NNX15AJ05A).

References

Ambaum, M. H. P. and Novak, L. (2014), A nonlinear oscillator describing storm track variability. Q.J.R. Meteorol. Soc., 140: 2680–2684. doi:10.1002/qj.2352.

Bauer, M., G. Tselioudis, and W. B,. Rossow, 2016: A new climatology for investigating storm infleunces in and on the extratropics, J. Appl. Meteor. Climatol., 55, 1287-1303.

Bernhardt J. E. and A. T. DeGaetano, 2012: Meteorological factors affecting the speed of movement and related impacts of extratropical cyclones along the U.S. east coast, *Nat. Haz.*, **61**, 1463-1472.

Bonazzi, A. , A. L. Dobbin, J. K. Turner, P. A. Wilson, C. Mitas, and E. Bellone (2014), A simulation approach for estimating hurricane risk over a 5-yr horizon, *Weather Clim. Soc.,* **6,** 77-90.

Booth, J. F., H. Reider, D. E. Lee, Y. Kushnir, 2015: The paths of extratropical cyclones associated with wintertime high wind events in the Northeast United States. *Journal of Applied Meterol. and Clim*. **54**, 1871-1885.

Born, K., P. L. Ludwig, and J. G. Pinto, 2012: Wind gust estimation for mid-European winter storms: Towards a probabilistic view. *Tellus*, **64A**, 17471, doi:10.3402/tellusa.v64i0.17471.

Cato, J. K., 2016: Extratropical cyclone classification and its use in climate studies. Rev. Geophys., 54, 486-520.

Colle, B. A., J. F. Booth, E. K. M. Chang, 2015: A review of historical and future changes of extratropical cyclones and associated impacts along the U.S. east coast. Current Climate Change Reports. *Current Climate Change Reports* **1**, 125-143.

573 Compo, G. P. and P. D. Sardeshmukh, 2004: Storm Track Predictability on Seasonal
574 and Decadal Scales. J. Climate 17, 3701–3720.
575 DeGaetano, A. T., M. E. Hirsch, and S. J. Colucci, 2002: Statistical prediction of
576 seasonal east coast winter storm frequency, *J. Clim*, 15, 1101-1117.
577 DeGaetano, A. T. 2008. Predictability of seasonal east coast winter storm surge
578 impacts with application to New York's Long Island. *Meteorological Applications,*
579 15**,** 231-242.
580 Dee D. P., et al., 2011: The ERA-Interim reanalysis: configuration and performance of
581 the data assimilation systems. *Quart. J. Roy. Meteor. Soc.,* **137**, 553-597.
582 Eichler, T., and W. Higgins, 2006: Climatology and ENSO-related variability of North
583 American extratropical cyclone activity, *J. Clim*., 19, 2076-2093.
584 Emanuel, K., E. Vivant, and C. Risi, 2006: A statistical deterministic approach of
585 hurricane risk assessment. *Bull. Amer. Meteor. Soc*, **87**, 299-314.
586 Gaffney, S.J., Robertson, A.W., Smyth, P., S. J. Camargo, M. Ghil, 2007: Probabilistic
587 clustering of extratropical cyclones using regression mixture models. . Clim Dyn
588 29-4 pp 423–440.
589 Grise, K. M., S.-W. Son, and J. R. Gyakum, 2013: Intraseasonal and interannual
590 variability in North American storm tracks and its relationship to equatorial
591 Pacific variability, *Mon. Wea. Rev*, 141, 3610-3625.
592 Hall, T. M., and S. Jewson, 2007: Statistical modeling of North Atlantic tropical
593 cyclone tracks, *Tellus*, 59A, 486-498.
594 Hall, T. M., and S. Jewson, 2008: Comparison of local and basinwide methods for risk
595 assessment of tropical cyclone landfall. *J. Appl. Meteor. Climatol*., **47**, 361-367.

596 Hall, T. M., and E. Yonekura, 2013: North American tropical cyclone landfall and SST:
597 A statistical model study, *J. Clim*., **26**, 8422-8439.
598 Haas, R., and J. G. Pinto, 2012: A combined statistical and dynamical approach for
599 downscaling large-scale footprints of European windstorms, *Geophys. Res. Lett*.,
600 **39**, L23804, doi:10.1029/2012GL054014.
601 He, Y., A. H. Monahan, C. G. Jones, A. Dai, S. Biner, D. Caya, and K. Winger, 2010:
602 Probability distributions of land surface wind speeds over North America. *J.*
603 *Geophys. Res.*, **115**, D04103, doi:10.1029/2008JD010708.
604 Hodges, K. I., R. W. Lee, L. Bengtsson, 2011: A Comparison of Extratropical Cyclones
605 in Recent Reanalyses ERA-Interim, NASA MERRA, NCEP CFSR, and JRA-25. *J.*
606 *Climate*, **24**, 4888–4906.
607 Hoskins, B. and K. Hodges, 2002: New Perspectives on the Northern Hemisphere
608 Winter Storm Tracks. *J. of Atmos. Sci.*, **59**, 1041-1061.
609 Hunter, A., D. B. Stephenson, T. Economou, M. Holland, and I. Cook, 2016: New
610 perspectives on the collective risk of extratropical cyclones. *Q. J. R. Meteorol. Soc*,
611 **142**, 243-256.
612 James, M. K., and L. B. Mason, 2005: Synthetic tropical cyclone database, *J. Waterw.*
613 *Port Coastal Ocean Eng*., **131**, 181-192.
614 Jones, P. D., T. Jonsson, and D. Wheeler, 1997: Extension of the North Atlantic
615 Oscillation using early instrumental pressure observations from Gibraltar and
616 South-West Iceland, *Int. J. Climatol*., 17, 1433-1430.

617 Klawa, M. and Ulbrich, U. 2003: A model for the estimation of storm losses and the
618 identification of severe winter storms in Germany, Nat. Hazard Earth Syst. Sci., 3,
619 725–732.
620 Kocin, P. J. and L. W. Uccellini, 2002: Snowstorms along the Northeastern Coast of
621 the United States, Volume I. Amer. Meteor. Soc., 280 pp.
622 Landsea, C., J. Franklin, and J. Beven, 2015: The revised Atlantic hurricane database
623 (HURDAT2), NHC NOAA, nhc.noaa.gov.
624 Miller. J. E., 1946: Cyclogenesis in the Atlantic coastal region of the United States. *J.*
625 *Meteor.* **3**, 31-44.
626 Neu, U., and Coauthors, 2013: IMILAST – a community effort to intercompare
627 extratropical cyclone detection and tracking algorithms: assessing method-
628 related uncertainties. *Bull. Am. Meteor. Soc.*, 94:529-547, doi:
629 http://dx.doi.org/10.1175/BAMS-D-11-00154.1
630 Ning, L., and R. S. Bradley, 2015: Winter climate extremes over the Northeastern
631 United States and Southeastern Canada and teleconnections with large-scale
632 modes of climate variability. *J. Clim*., 28, 2475-2493.
633 Orton, P. M., T. M. Hall, S. A. Talke, A. F. Blumberg, N. Georgas, and S. Vinogradov,
634 2016: A validated tropical-extratropical flood hazard assessment for New York
635 Harbor, *J. Geophys. Res*., in press..
636 Pinto, J. G., S. Zacharias, S., A. H. Fink, G. C. Leckebusch, U. Ulbrich, 2009: Factors
637 contributing to the development of extreme North Atlantic cyclones and their
638 relationship with the NAO. *Clim. Dyn*., **32**, 711–737.

639 Plante, M., S.-W. Son, E. Atallah, J. Gyakum, and K. Grise, 2015: Extratropical cyclone
640 climatology across eastern Canada, *Inter. J. Clim*., 10, 2759-2776.
641 Rayner, N. A., D. E. Parker, E. B. Horton. C. K. Folland, L. V. Alexander, D. P. Rowell, E.
642 C. Kent, and A. Kaplan, 2003: Global analysis of sea surface temperature, sea ice,
643 and night marine air temperature since the late nineteenth century, *J. Geophys.*
644 *Res.*, 108 (D14), 4407, doi:10.1029/2002JD002670.
645 Rumpf, J. H. Weindl, P. Hoppe, E. E. Raughe, and V. Schmidt, 2007: Stochastic
646 modeling of tropical cyclone tracks. *Math Methods Oper. Res*., **66**, 475-490.
647 Sanders, F. and J. R. Gyakum, 1980: Synoptic-Dynamic climatology of the "bomb".
648 *Mon. Wea. Rev.*, **108**, 1589-1606.
649 Seregina, L. S., R. Haas, K. Born, J. G. Pinto, 2014: Development of a wind gust model
650 to estimate gust speeds and their return periods. *Tellus A* **66**, 22905.
651 doi:10.3402/tellusa.v66.22905
652 Serreze, M. C., F. Carse, R. G Barry, and J. C. Rogers, 1997: Icelandic low cyclone
653 activity: climatological features, linkages with the NAO, and relationships with
654 recent changes in the Northern Hemisphere circulation. *J. Climate*, **10**, 453-464.
655 Smith, A. B., and R. W. Katz, 2013: US billion-dollar weather and climate disasters:
656 data sources, trends, accuracy and biases, *Natural Hazards*, 67, 387-410.
657 Ulbrich U, Leckebusch GC, Pinto JG (2009) Extra-tropical cyclones in the present and
658 future climate: A review. *Theor Appl Climatol,* **96**,117–131
659 Vickery, P., P. Skerij, and L. Twisdale, 2000: Simulation of hurricane risk in the U.S.
660 using empirical track model, *J. Struct. Eng.,* **126**, 1222-1237.

661 Vose, R.S., et al. 2014: Monitoring and understanding changes in extremes: extratropical
662 storms, winds, and waves. Bulletin of the American Meteorological Society 95:377-
663 386, doi:10.1175/BAMS-D-12-00162.1.
664 Yang, X., G. A. Vecchi, T. L. Delworth, K. Paffendorf, R. Gudgel, L. Jia, S. Underwood,
665 and F. Zeng, 2015: Extreme North American winter storm season of 2013/14:
666 Roles of radiative forcing and the global warming hiatus 9in "Explaining Extremes
667 of 2014 from a Climate Perspective"] *Bull. Amer. Meteor. Soc.*, 96(12), S25-S28.
668 Yonekura, E., and T. M. Hall, 2014: ENSO effect on East Asian tropical cyclone
669 landfall via changes in tracks and genesis in a statistical model. *J. Appl. Meteoolr.*
670 *Clim*., **53**, 406-420.
671
672 **Fig 1:** ETC tracks 1979-2015 whose intensity (local SLP climatology minus central
673 pressure) reach at least 35mb. Tracks are color coded by intensity: any intensity
674 (blue), greater than 30mb (yellow), and greater than 50mb (red). There are 1782
675 tracks. Light blue circles indicate evaluation regions of 200km radius about the
676 following nine cities used in figures below: New York, Boston, Washington DC,
677 Toronto, Chicago, Detroit, Duluth, Montreal, and Halifax.
678
679 **Fig 2:** Monthly histograms of 1979-2015 ETCs in the full set (purple), minus tropical
680 cyclones (blue), and ETCs whose intensity somewhere reaches at least 35mb (red).
681
682 **Fig 3:** Space-date kernel density formation pdf of ETCs that have 35mb+ intensity
683 somewhere during their lifetime. The pdf is used to place simulated ETC formation

684 events in the year. It has time interval of pentads, and fields at central pentads of the
685 months are shown. The contours are in units of counts per pentad per 1°-by-1°
686 longitude-latitude box.
687
688 **Fig 4:** Illustration of the model's track component: a four-day mean track for Jan 15
689 conditions (red) released from 72°W, 36°N; and a set of 1000 track simulations
690 including the stochastic component (gold) released from the same point. Also shown
691 are historical tracks originating from within 175km of 72°W, 36°N. In the
692 simulations NAO = -0.4 and ENSO = -0.3, the mean standardized anomaly values for
693 historical ETC originating from the 175km-radius region.
694
695 **Fig 5:** Example of intensity time series sampling. Left: A historical target track on
696 which to place an intensity series, selected from 2012 (blue), the sub-set of tracks
697 from 1979-2015 excluding 2012 that have at least a 0.001 sampling probability
698 according to the track-similarity criteria (thin red), and the most probable track
699 (thick red). For this example the most probable track has a selection probability of
700 0.45, while the next three highest probabilities are 0.23, 0.20, and 0.04. Right: The
701 intensity time series that correspond to the tracks, plotted versus day from
702 formation, including the most likely sampled (thick red) and the out-of-sample
703 historical (blue) for comparison. The sampled series have been scaled in time to
704 match the duration of the target track.
705

706 **Fig 6:** Four simulations of 1979-2015 colored coded by intensity: all tracks (blue),
707 30mb+ (yellow), and 50mb+ (red).
708
709 **Fig. 7**: Three examples of simulated ETCs more extreme than any ETC occurring in
710 the 1979-2015 historical record. They pass within 200km of Washington DC, New
711 York City, and Boston, as labeled, with intensity greater than 60mb. Color intervals
712 are units of mb.
713
714 **Fig 8:** Number of 1979-2015 tracks crossing six lines of constant longitude in 5°
715 latitude bins (left) and six lines of constant latitude in 5° longitude bins (right).
716 Eastward crossing (left) is indicated by the rightward bulge and northward crossing
717 (right) by the upward bulge. Units are counts per 5° latitude (left) and longitude
718 (right) accumulated over 1979-2015, and the flux magnitudes are indicated by the
719 bar lengths in the upper left of each panel. Red curves represent crossings of the
720 historical track set. Dark blue represents the inner 90% across the ensemble of
721 1979-2015 simulations. Vertical and horizontal dashed lines indicate zero flux and
722 are shown for reference.
723
724 **Fig 9:** Intensity as a function of return period of ETCs whose centers pass within
725 200km of the cities labeled here and indicated in Fig 1. The blue curves are obtained
726 directly from the 1979-2015 historical data, the orange curves indicate the 5% and
727 95% across 1000 simulations of 1979-2015. Red is obtained from placing the 1000
728 simulations in series, resulting in a 37,000-year simulation.

729

730 **Fig 10:** Annual rate of an ETC with 50mb+ intensity passing within 200km as a
731 function of ENSO and NAO as labeled in standardized units. Contour units are yr^{-1}.

732

733 **Fig 11:** Fractional change in annual rate of an ETC with 50mb+ intensity passing
734 within 200km compared to the neutral state as a function of ENSO and NAO as
735 labeled. Contours are fractional difference from the neutral state. Values are plotted
736 only where the annual rate is greater than 0.01.

737

738 **Fig 12:** Formation rate ratios of the specified ENSO-NAO state to the neutral state
739 for Jan 15. Values are plotted only where the rate is greater than 5% of its
740 geographic maximum. Contours are fractional difference from the neutral state.

741

742 **Fig 13:** Mean tracks (track simulations without the stochastic component) have
743 identical fixed durations of four days originating from three locations at nine ENSO-
744 NAO states for Jan 15. In each panel red curves represent the mean tracks for the
745 specified ENSO-NAO state, and blue curves represent the neutral state shown for
746 reference.

747

748 **Fig 14:** Annual occurrence rate of an ETC with 50mb+ intensity within 200km of
749 New York City (left) and Duluth MN (right) as functions of ENSO and NAO. The
750 minimum to maximum range for New York City is 0.012-0.05 yr^{-1} and for Duluth is
751 0.004-0.03 yr^{-1}.

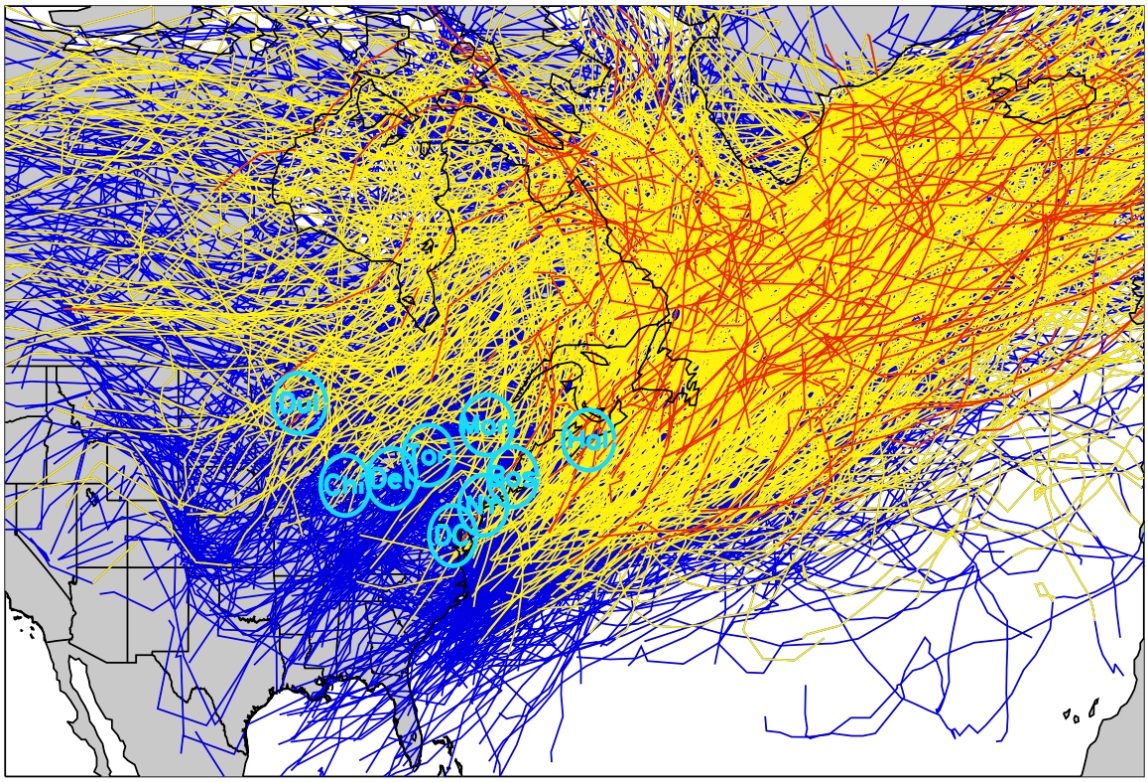

752

753 **Fig 1:** ETC tracks 1979-2015 whose intensity (local SLP climatology minus central
754 pressure) reach at least 35mb. Tracks are color coded by intensity: any intensity
755 (blue), greater than 30mb (yellow), and greater than 50mb (red). There are 1782
756 tracks. Light blue circles indicate evaluation regions of 200km radius about the
757 following nine cities used in figures below: New York, Boston, Washington DC,
758 Toronto, Chicago, Detroit, Duluth, Montreal, and Halifax.

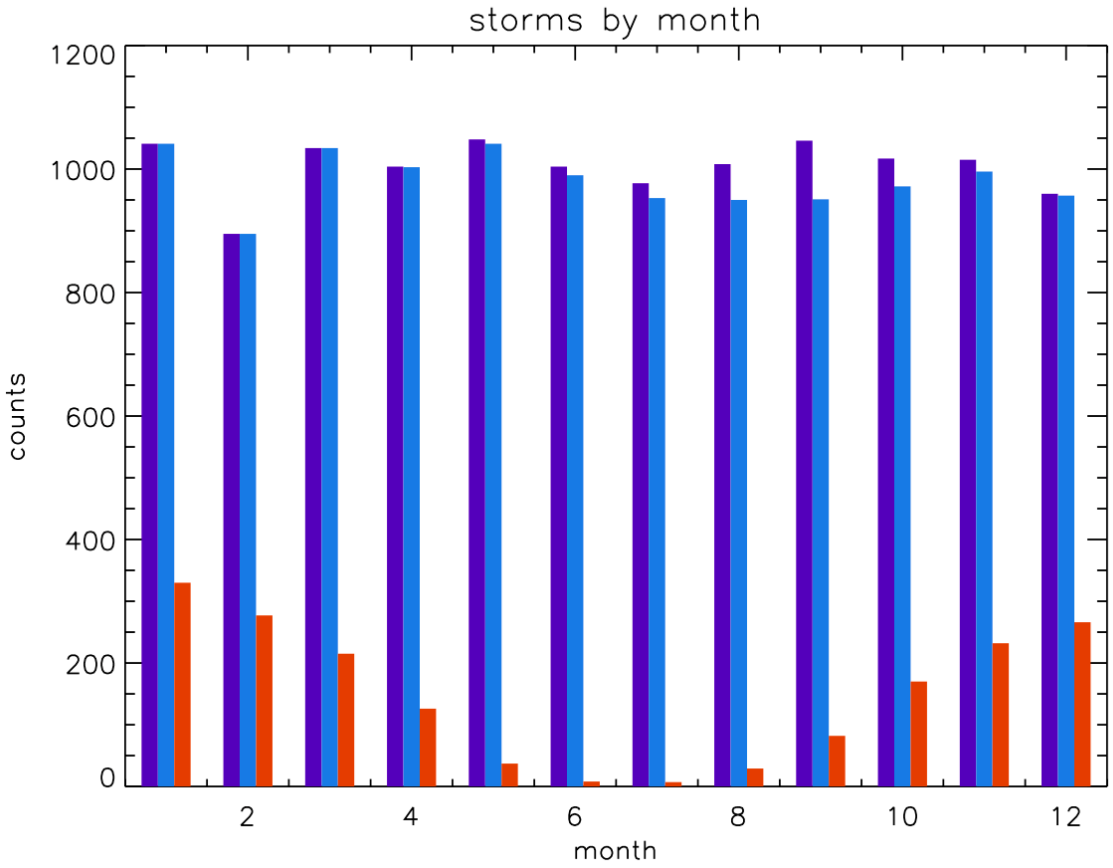

759

760

761 **Fig 2:** Monthly histograms of 1979-2015 ETCs in the full set (purple), minus tropical

762 cyclones (blue), and ETCs whose intensity somewhere reaches at least 35mb (red).

763

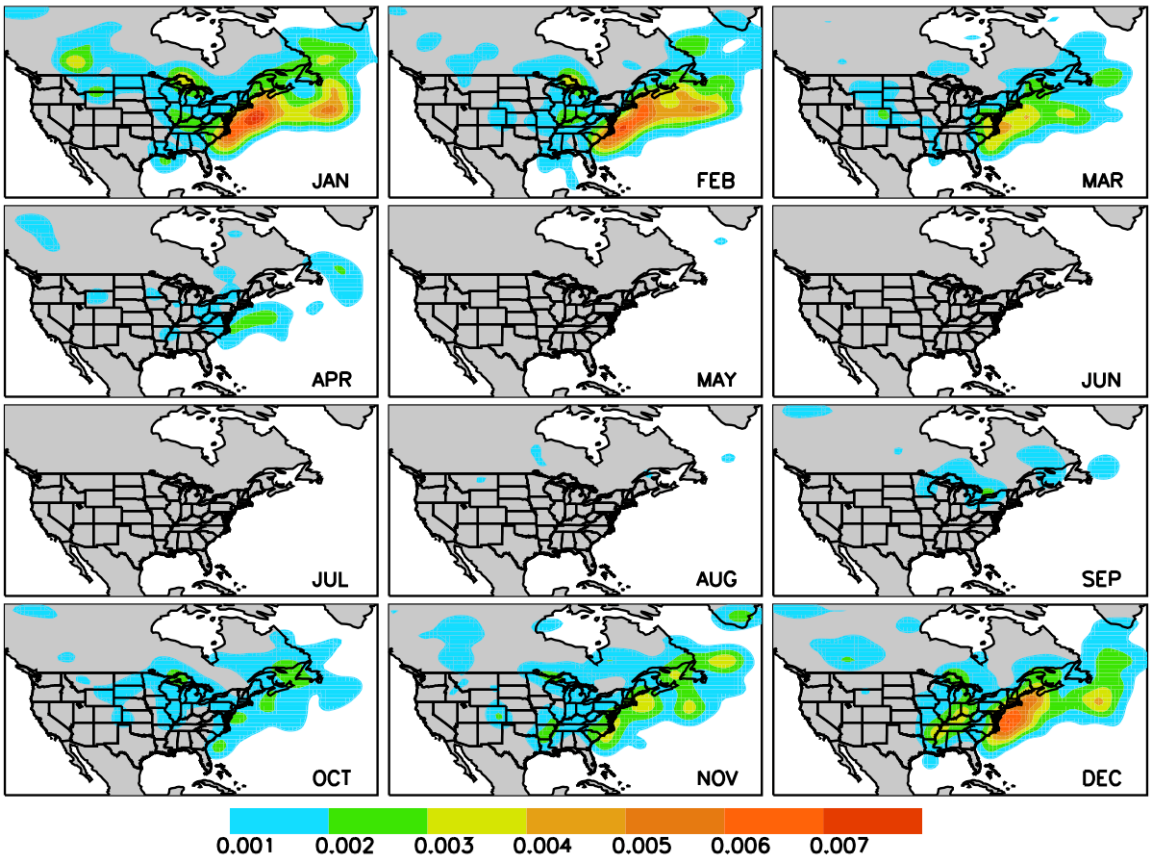

764

765

766 **Fig 3:** Space-date kernel density formation pdf of ETCs that have 35mb+ intensity
767 somewhere during their lifetime. The pdf is used to place simulated ETC formation
768 events in the year. It has time interval of pentads, and fields at central pentads of the
769 months are shown. The contours are in units of counts per pentad per 1°-by-1°
770 longitude-latitude box.

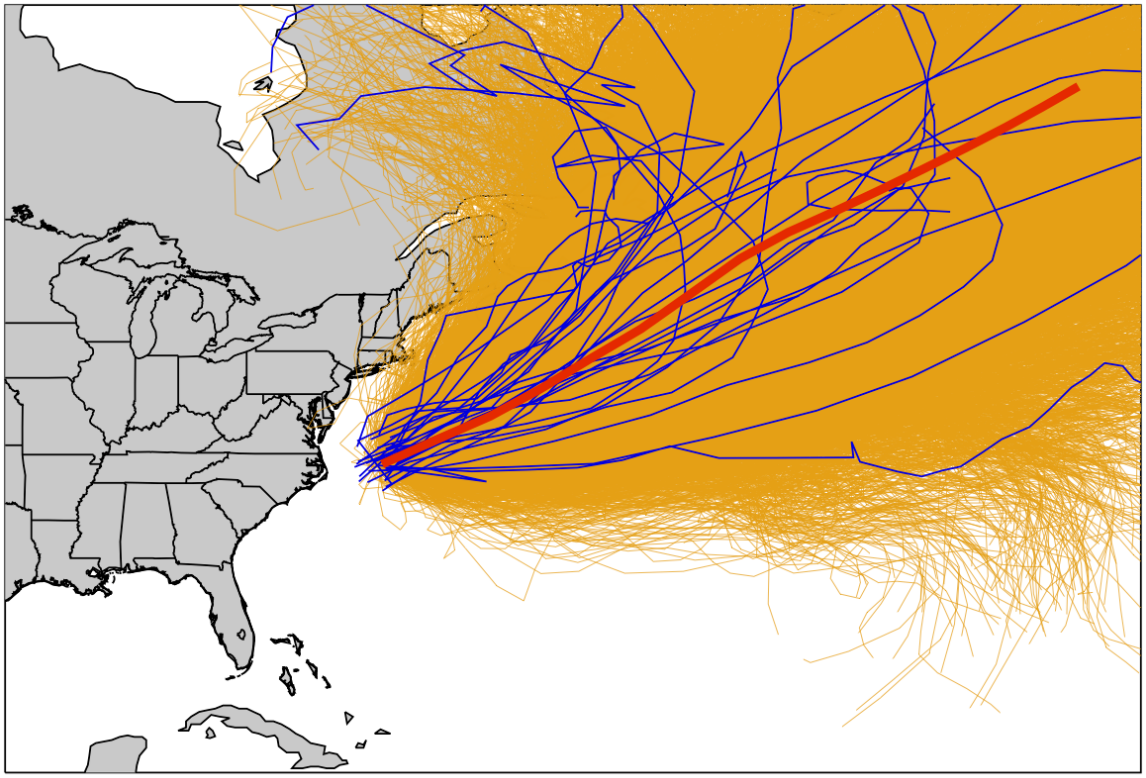

Fig 4: Illustration of the model's track component: a four-day mean track for Jan 15 conditions (red) released from 72°W, 36°N; and a set of 1000 track simulations including the stochastic component (gold) released from the same point. Also shown are historical tracks originating from within 175km of 72°W, 36°N. In the simulations NAO = -0.4 and ENSO = -0.3, the mean standardized anomaly values for historical ETC originating from the 175km-radius region.

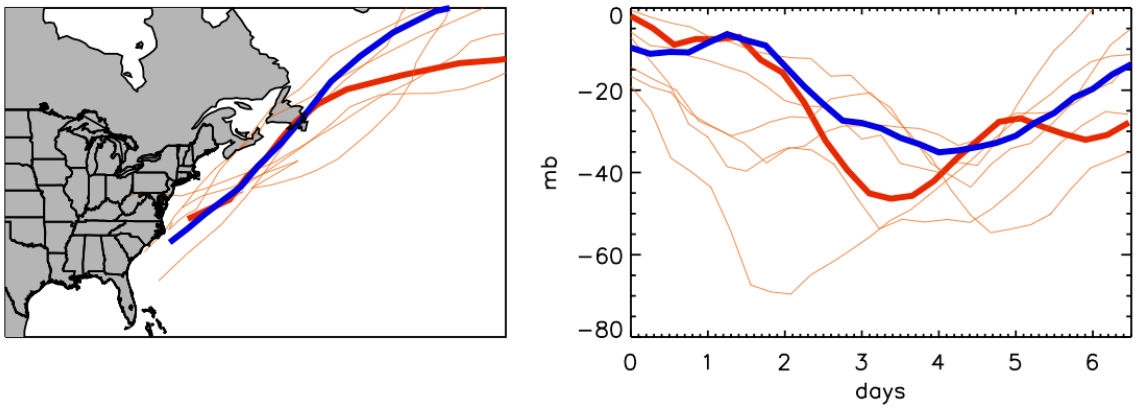

779

780 **Fig 5:** Example of intensity time series sampling. Left: A historical target track on
781 which to place an intensity series, selected from 2012 (blue), the sub-set of tracks
782 from 1979-2015 excluding 2012 that have at least a 0.001 sampling probability
783 according to the track-similarity criteria (thin red), and the most probable track
784 (thick red). For this example the most probable track has a selection probability of
785 0.45, while the next three highest probabilities are 0.23, 0.20, and 0.04. Right: The
786 intensity time series that correspond to the tracks, plotted versus day from
787 formation, including the most likely sampled (thick red) and the out-of-sample
788 historical (blue) for comparison. The sampled series have been scaled in time to
789 match the duration of the target track.

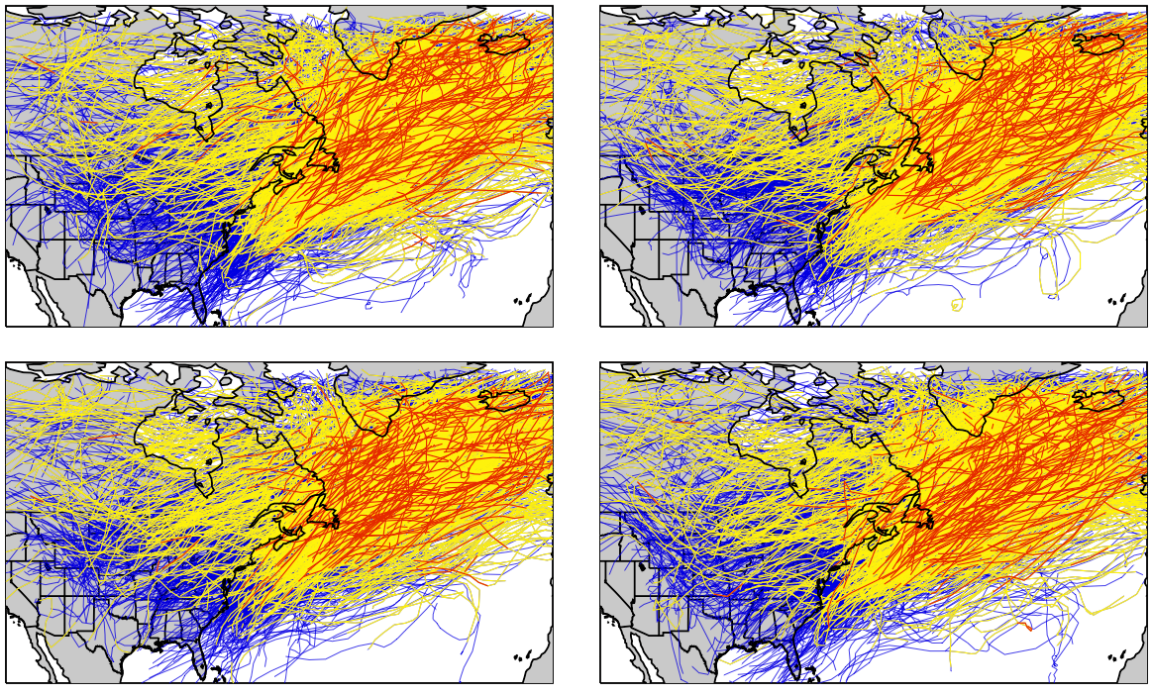

Fig 6: Four simulations of 1979-2015 colored coded by intensity: all tracks (blue), 30mb+ (yellow), and 50mb+ (red).

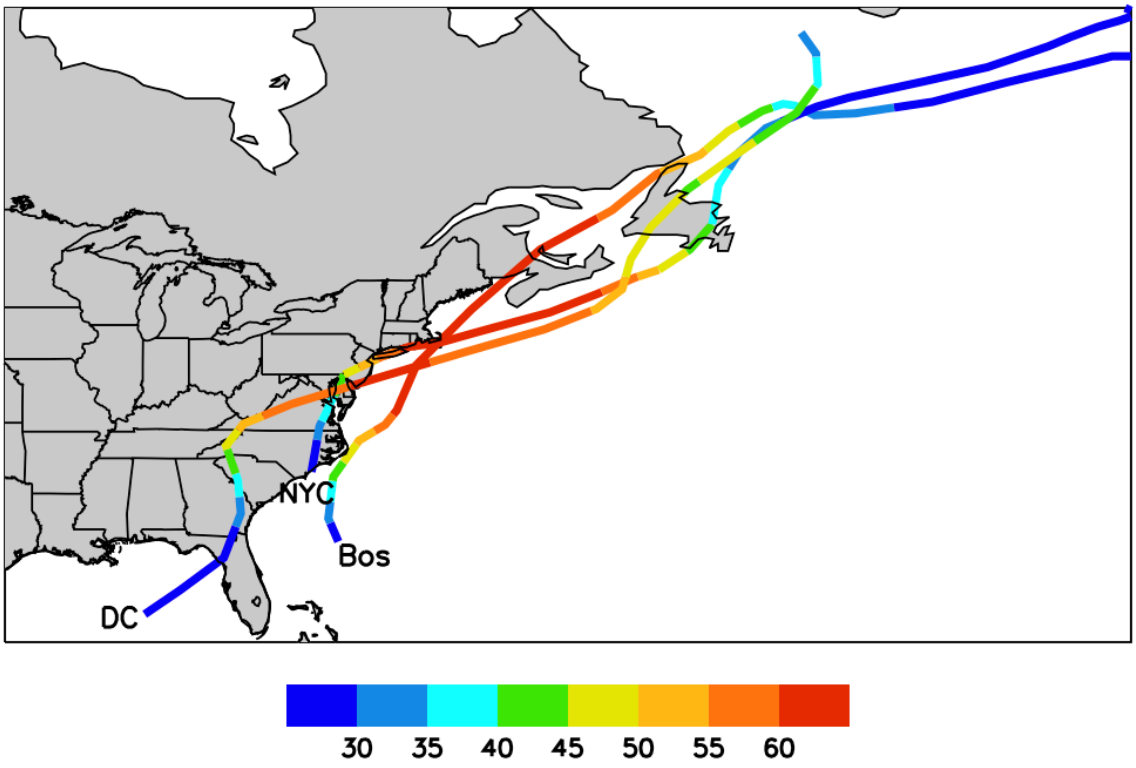

794

795 **Fig. 7**: Three examples of simulated ETCs more extreme than any ETC occurring in

796 the 1979-2015 historical record. They pass within 200km of Washington DC, New

797 York City, and Boston, as labeled, with intensity greater than 60mb. Color intervals

798 are units of mb.

799

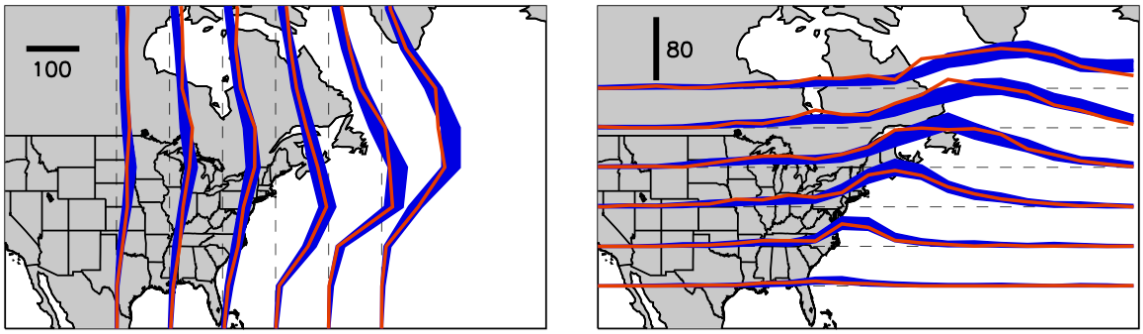

Fig 8: Number of 1979-2015 tracks crossing six lines of constant longitude in 5° latitude bins (left) and six lines of constant latitude in 5° longitude bins (right). Eastward crossing (left) is indicated by the rightward bulge and northward crossing (right) by the upward bulge. Units are counts per 5° latitude (left) and longitude (right) accumulated over 1979-2015, and the flux magnitudes are indicated by the bar lengths in the upper left of each panel. Red curves represent crossings of the historical track set. Dark blue represents the inner 90% across the ensemble of 1979-2015 simulations. Vertical and horizontal dashed lines indicate zero flux and are shown for reference.

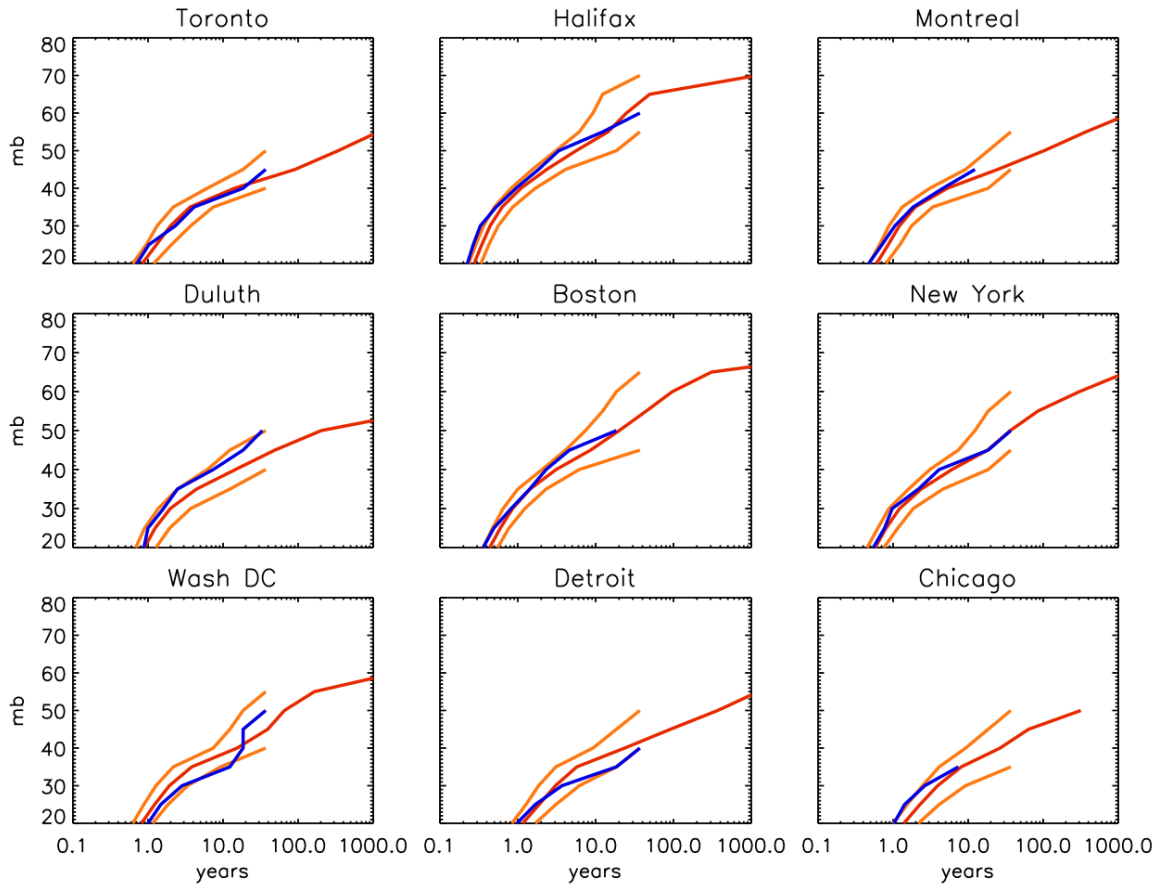

811

812 **Fig 9:** Intensity as a function of return period of ETCs whose centers pass within
813 200km of the cities labeled here and indicated in Fig 1. The blue curves are obtained
814 directly from the 1979-2015 historical data, the orange curves indicate the 5% and
815 95% across 1000 simulations of 1979-2015. Red is obtained from placing the 1000
816 simulations in series, resulting in a 37,000-year simulation.

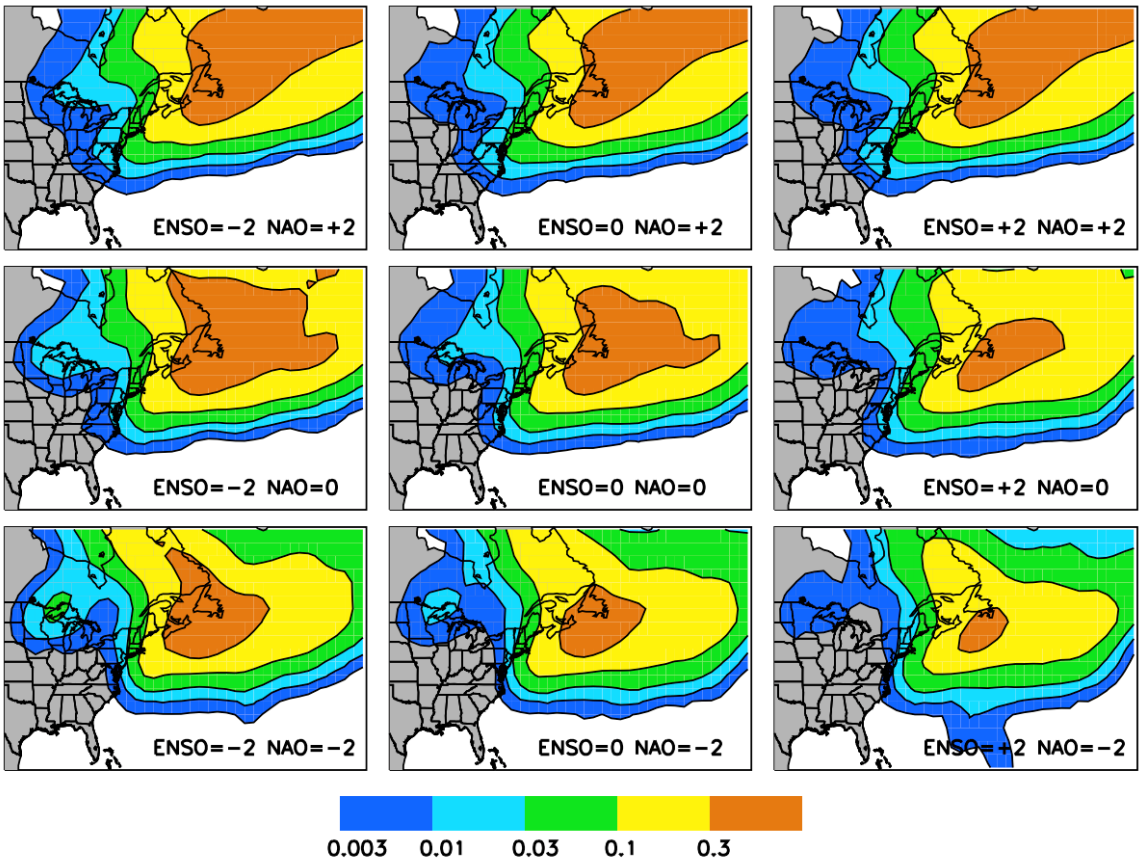

817

818 **Fig 10:** Annual rate of an ETC with 50mb+ intensity passing within 200km as a

819 function of ENSO and NAO as labeled in standardized units. Contour units are yr^{-1}.

820

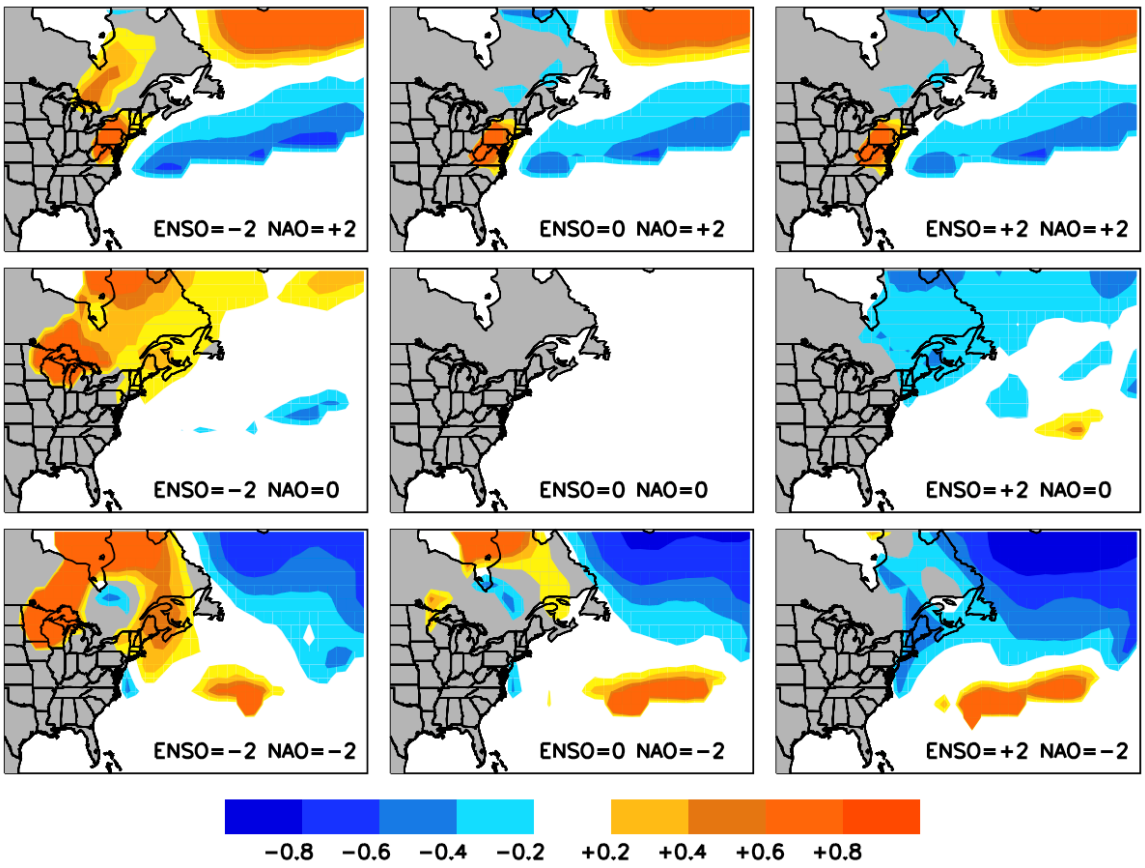

821

822 **Fig 11:** Fractional change in annual rate of an ETC with 50mb+ intensity passing
823 within 200km compared to the neutral state as a function of ENSO and NAO as
824 labeled. Contours are fractional difference from the neutral state. Values are plotted
825 only where the annual rate is greater than 0.01.

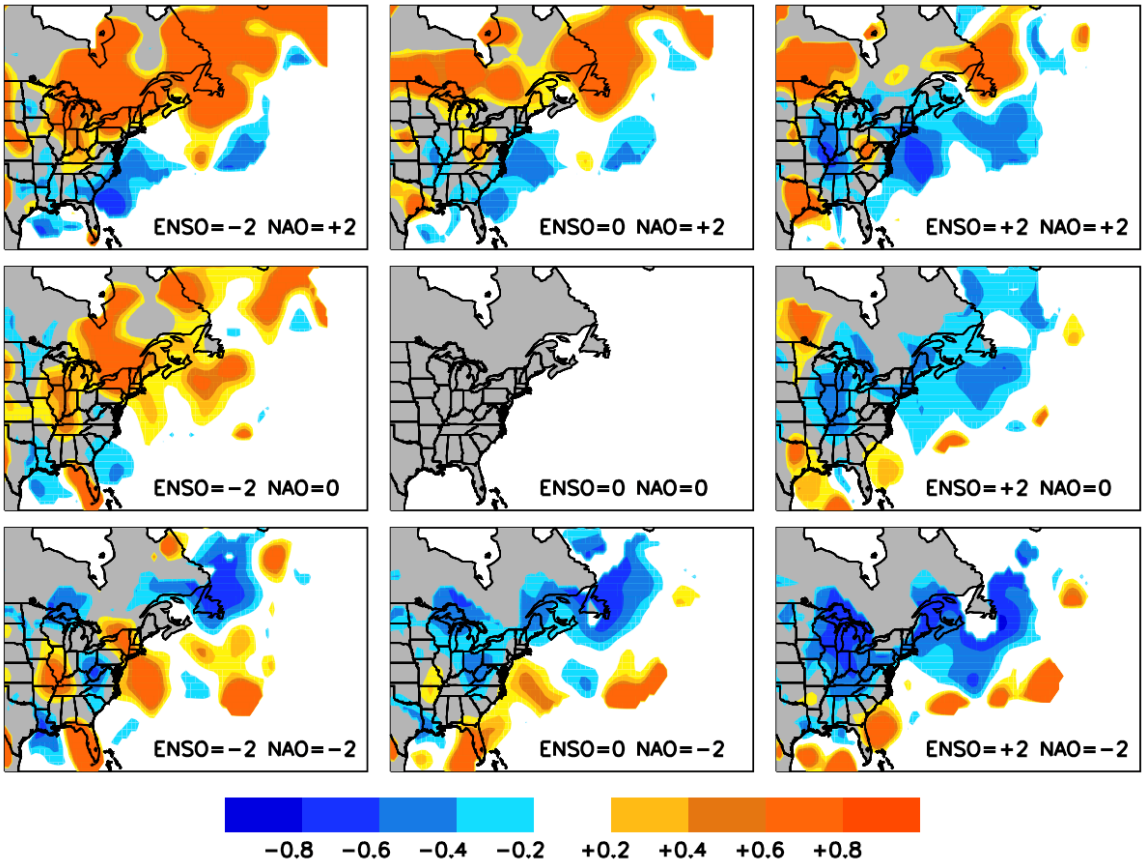

826

827 **Fig 12:** Formation rate ratios of the specified ENSO-NAO state to the neutral state

828 for Jan 15. Values are plotted only where the rate is greater than 5% of its

829 geographic maximum. Contours are fractional difference from the neutral state.

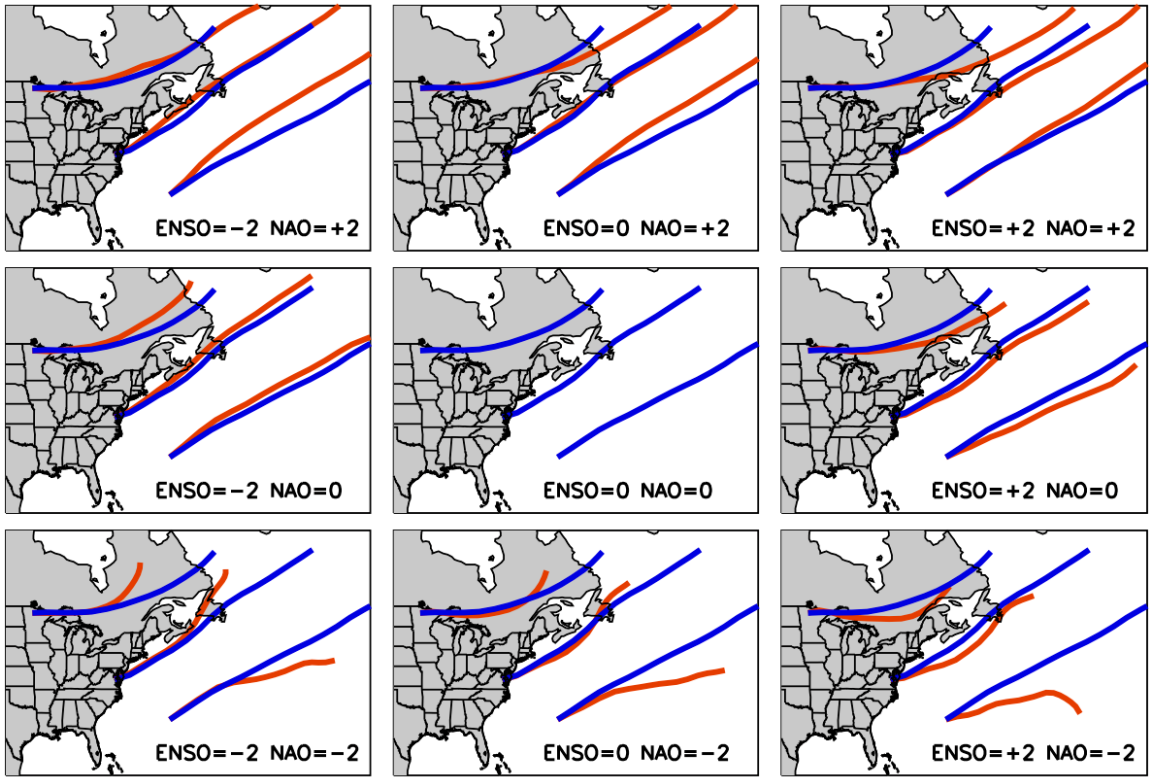

Fig 13: Mean tracks (track simulations without the stochastic component) have identical fixed durations of four days originating from three locations at nine ENSO-NAO states for Jan 15. In each panel red curves represent the mean tracks for the specified ENSO-NAO state, and blue curves represent the neutral state shown for reference.

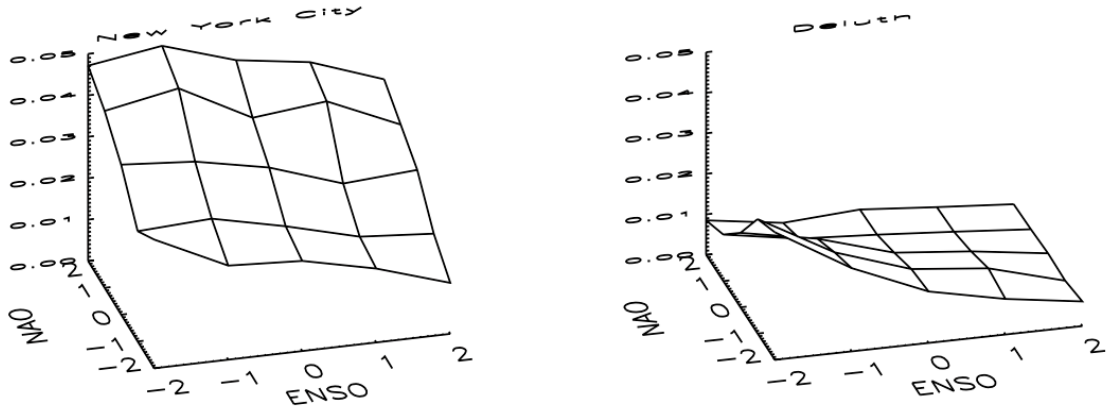

Fig 14: Annual occurrence rate of an ETC with 50mb+ intensity within 200km of New York City (left) and Duluth MN (right) as functions of ENSO and NAO. The minimum to maximum range for New York City is 0.012-0.05 yr^{-1} and for Duluth is 0.004-0.03 yr^{-1}.